Demystifying T1-MRI to FDG^{18}-PET Image Translation via Representational Similarity

Chia-Hsiang Kao, Yong-Sheng Chen, Li-Fen Chen, and Wei-Chen Chiu[†]

National Yang Ming Chiao Tung University, Taiwan
[†]walon@cs.nctu.edu.tw

Abstract. Recent development of image-to-image translation techniques has enabled the generation of rare medical images (e.g., PET) from common ones (e.g., MRI). Beyond the potential benefits of the reduction in scanning time, acquisition cost, and radiation exposure risks, the translation models in themselves are inscrutable black boxes. In this work, we propose two approaches to demystify the image translation process, where we particularly focus on the T1-MRI to PET translation. First, we adopt the representational similarity analysis and discover that the process of T1-MR to PET image translation includes the stages of brain tissue segmentation and brain region recognition, which unravels the relationship between the structural and functional neuroimaging data. Second, based on our findings, an Explainable and Simplified Image Translation (ESIT) model is proposed to demonstrate the capability of deep learning models for extracting gray matter volume information and identifying brain regions related to normal aging and Alzheimer's disease, which untangles the biological plausibility hidden in deep learning models.

Keywords: Explainability · Medical image translation.

1 Introduction

Recent advances in deep learning have brought the magic leap to various research areas such as computer vision and natural language processing. In these days, we have witnessed the great performance of deep learning models [27,18,26] for making translation from T1-weighted magnetic resonance (T1-MR) images towards 18-fluorodeoxyglucose proton emission tomography images (FDG^{18}-PET) (FDG^{18}-PET is abbreviated to PET unless stated otherwise). Typically, the T1-MR imaging, a type of structural magnetic resonance imaging (MRI) scan, is an anatomical image used to observe the brain structures, thus being known as one of the *structural imaging*; while PET studies the *in vivo* glucose metabolism, which is correlated with neuronal activity and stimulus intensity [24], thus being defined as *functional imaging*. Yet these two imaging techniques are different in terms of their physical and biological characteristics, it remains unexplored to understand the mechanism behind deep-learning-based translation models of bridging the difference between structural and functional images, in which it motivates us to demystify such image translation process, as the main goal

of this paper. The basic idea behind our research framework is illustrated in Figure 1.

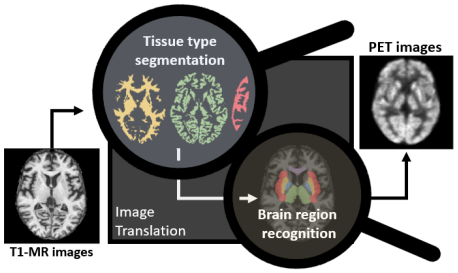

Fig. 1: We propose to lay the explanatory groundwork for the cross-modal medical image translation model by exploring the biological plausibility behind the deep neural net. We experimentally validate our proposed hypotheses that the T1-MR to PET translation comprises successive recognition of the brain tissue types and the brain regions.

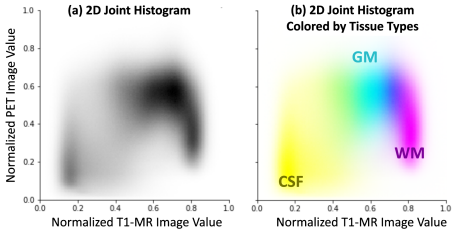

Fig. 2: Figure (a) shows the 2D joint histogram of values from corresponding T1-MR and PET image pixels, while it is further colorized by the probability of pixels belonging to different tissue types (i.e., white matter (WM) be purple, gray matter (GM) be cyan, and CSF be yellow) and shown in (b).

Our study begins with building a 2D joint histogram between the values obtained from the corresponding T1-MR and PET image pixels. In Figure 2, we observe three clusters which are associated to cerebro-spinal fluid (CSF) and brain tissues. We therefore have our first hypothesis: during image translation, the model would first recognize (or segment) the areas related to various brain tissue types. Nevertheless, as these clusters are not compact and their boundaries are blurry, merely having the tissue regions as the intermediary can not conclusively reason the translation between images. We hence step further and hypothesize: as different brain regions (e.g., thalamus, insula, or putamen) have different baseline uptake of glucose, there would be an in-between stage of brain regions identification followed by performing region-dependent transformation.

We experimentally verify our hypotheses using the representational similarity analysis, thus contributing to decipher the black box translation model. Moreover, we advance to leverage these two hypotheses by building up an **Explainable and Simplified Image Translation (ESIT)** model. With ESIT model, we look into its learnt feature representations and discover their close relationship with the gray matter volume as well as the informativeness on clinical status.

2 Related Works

Image Translation in Medical Domains. Image-to-image translation is the task of transforming the images from one domain to the ones of another domain

with distinct characteristics/styles, i.e. mapping between image domains. Several approaches [17,18,25,26,10] have been proposed to translate images from T1-MR to PET, where most of them are based on U-Net architecture [21] with using the paired data (i.e. cross-domain correspondences). Instead of pushing forward the model performance on T1-MR to PET image translation, our primary goal is to explore the underlying mechanism of deep-learning-based translation methods. Therefore, our research focuses on the typical U-Net structure that is widely used as a building block for various translation models.

Analysis of Representational Similarity for Deep Networks. To better characterize deep learning models, various methods have been proposed to analyze the optimization process or the internal organization of neural networks, such as filter visualization [29,28] or saliency maps [1,22]. However, as these approaches are developed mainly for classification models, their direct application on image-to-image translation models is challenging since the high-dimensional structural and semantic information are substantially entangled during translation. Recently, *Canonical Correlation Analysis* (CCA) has emerged as a robust tool to study the similarity of representations within a deep network or across networks, as CCA measures the multivariate joint relationship among variables/representations via maximizing the correlation between their projections. In our study, we take advantage of CCA to calculate the per-layer representational similarity scores with respect to brain tissue maps and brain region templates.

3 Image Translation Model, Dataset, and Analysis Tool

As motivated previously, we propose to analyze the trained U-Net model of T1-MR to PET image translation by exploring its layer-wise representational similarity with respect to medically interpretable concepts, i.e., the brain tissue maps and the brain region templates. In this section, we provide the details of the U-Net model, the dataset in use, and CCA as our analysis tool.

U-Net Model for T1-MR to PET Image Translation. As the basis for our study, we start off with training the U-Net model for performing image translation from T1-MR to PET images. We adopt the typical U-Net architecture proposed in [21] but substitute its batch normalization, ReLU activation, and those convolution layers followed by the maxpooling operation with the instance normalization (IN), Leaky ReLU (LR) activation, and strided convolution layers, respectively. Such U-Net model is trained to minimize the L1 loss with AdamW optimizer [11] for 40 epochs over five-fold cross-validation. The quantitative metrics used for evaluating the translation performance are mean square error (MAE), peak signal-to-noise ratio (PSNR), and structure similarity index (SSIM).

Alzheimer's Disease Neuroimaging Initiative Dataset. The paired T1-MR and PET images are obtained from the Alzheimer's Disease Neuroimaging Initiative dataset (ADNI [9]) including ADNI-1, ADNI-2, ADNI-GO, and ADNI-3 phases. Overall, we include the data of cognitively normal (CN, n=300) subjects

and subjects diagnosed as significant memory concern (SMC, n=54), mild cognitive impairment (MCI, n=868) and Alzheimer's disease (AD, n=219).

Preprocessing. We follow standard procedure to perform image preprocessing using the SPM 12 software [19]. PET images are coregistered to the corresponding T1-MR images. Then, T1-MR images are transformed to Montreal Neurological Institute (MNI) reference space with the voxel size resliced to $1.5\times1.5\times1.5\ mm^3$, and the estimated deformation field is applied to the aligned PET images. Skull-stripping and cerebellum removal are performed to all PET images as indicated in [18]. Min-Max normalization of pixel values to the range $[0, 1]$ is performed to all T1-MR images and PET images.

Brain Tissue Maps and Brain Region Templates. The subject-specific probabilistic maps of gray matter (GM), white matter (WM) and CSF are obtained from the T1-MR image segmentation by SPM. For brain region templates, we utilize Automated Anatomical Labeling (AAL3) [20] and Hammersmith atlas [8], which are resliced to match the spatial resolution of T1-MR images.

Canonical Component Analysis. Canonical Component Analysis (CCA) measures the relationship between two variables by finding a canonical space in which the correlation between their projections onto that space is maximized. Given two centered random vectors $\mathbf{X}$ and $\mathbf{Y}$ of dimensions m and n respectively, where $\mathbf{X} = (x_1, ..., x_m)^T$ and $\mathbf{Y} = (y_1, ..., y_n)^T$, CCA seeks pairs of projection weight vectors $\mathbf{a}_i \in \mathbb{R}^m$ and $\mathbf{b}_i \in \mathbb{R}^n$ iteratively to maximize the correlation coefficient between $\mathbf{a}_i^T\mathbf{X}$ and $\mathbf{b}_i^T\mathbf{Y}$, under the orthogonality constraints that $\forall j < i, \mathbf{a}_i^T\mathbf{X} \perp \mathbf{a}_j^T\mathbf{X}$ and $\mathbf{b}_i^T\mathbf{Y} \perp \mathbf{b}_j^T\mathbf{Y}$. For $1 \leq i \leq \min(m, n)$, the i^{th} canonical correlation coefficient ρ_i is therefore given by:

$$\rho_i = \max \frac{< \mathbf{u}_i, \mathbf{v}_i >}{\|\mathbf{u}_i\|\|\mathbf{v}_i\|} = \max \frac{(\mathbf{a}_i^T\mathbf{X})(\mathbf{b}_i^T\mathbf{Y})^T}{\|\mathbf{a}_i^T\mathbf{X}\|\|\mathbf{b}_i^T\mathbf{Y}\|} \tag{1}$$

where $\mathbf{u}_i = \mathbf{a}_i^T\mathbf{X}$ and $\mathbf{v}_i = \mathbf{b}_i^T\mathbf{Y}$ are called *canonical components*.

In details, the activation maps from a network are concatenated along spatial dimension to form $d \times h \times w$ vectors with dimension c, denoted by $\mathbf{L}$ (where d, h, w, c are respectively the number of datapoint, height, width, and the number of channels). The brain tissue maps and the brain region templates are flattened into $d \times h \times w$ vectors with dimension 1, denoted by $\mathbf{K}$. We use CCA to find the projection weight vectors $\mathbf{w}_1 \in \mathbb{R}^c$ and $\mathbf{w}_2 \in \mathbb{R}^1$, such that the correlation coefficient $\rho = \max \frac{(\mathbf{w}_1^T\mathbf{L})(\mathbf{w}_2^T\mathbf{K})^T}{\|\mathbf{w}_1^T\mathbf{L}\|\|\mathbf{w}_2^T\mathbf{K}\|}$ is maximized.

We name the correlation coefficient ρ as ***CCA similarity***, since such values reflect the degree of correlation between two random variables in a canonical coordinate space. To avoid interference by zero-valued regions (i.e., pixels of air and bone), we remove the data point which is neither brain tissues nor CSF. Due to the expensive computational cost, for each model, we randomly sample 20 subjects from corresponding training data and retrieve their activation maps

of every layer (after Leaky ReLU operator) from the translation model. The standard deviation of the CCA similarities is plotted as the shaded region.

4 Demystification from a Medical Perspective

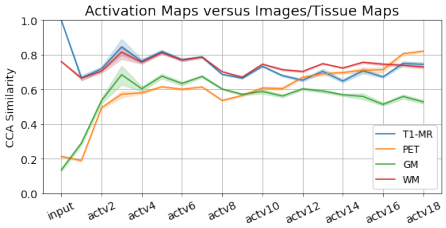

(a) CCA similarity of activation maps against T1-MR images, PET images, and brain tissue maps. Please refer to Section 4.1 for more detailed discussion.

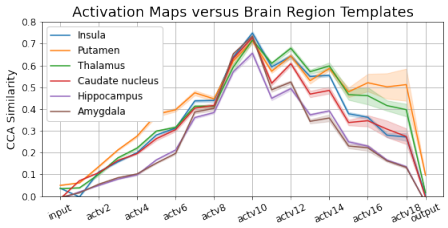

(b) CCA similarities between the per-layer activation maps and the brain region templates. Please refer to Section 4.3 for more detailed discussion.

Fig. 3: Per-layer CCA similarity scores of per-layer activation maps

4.1 Brain Tissues Are Segmented in the Early Encoding Stage

To verify our first hypothesis that, during the translation process, the translation model would first recognize the areas related to brain tissue types, our work begins with showing the CCA similarity scores of per-layer activation maps with respect to the brain tissue maps and the T1-MR/PET images, as provided in Figure 3a. We have several observations: (1) The increase of CCA scores between the activation maps and the gray matter maps (i.e., the curve in green color) in the early encoding stage (i.e., from layer *actv1* to *actv3*), indicating that the translation model learns to recognize the gray matter distribution; (2) In the encoding stage, the trend of CCA similarity between the activation maps and the gray matter maps is similar to the one between the activation maps and the PET images (i.e., the curve in orange color). Such observation echoes the physical principle [13] that gray matter has higher metabolic activity, which PET imaging aims to capture. To further understand the information captured by the translation model, we show the canonical components of the *actv3* activation maps in Figure S1 of supplement, which highly resemble the tissue maps.

4.2 Brain Tissue Information Is the Key to PET Image Synthesis

Based on our observation that the translation model learns to represent the tissue type information in the early encoding stage, we wonder if the tissue information alone is sufficient for PET image synthesis. As shown in the first two columns in

Table S1 of supplement, the performance of the U-Net-based translation model which is directly trained on tissue maps as input is competitive to the original translation model (i.e., trained by taking T1-MR images as input), verifying our assumption that the brain tissue information is the key to PET image synthesis.

4.3 Brain Regions Are Recognized Later in the Translation

In Figure 3a, we observe a steady increase in the per-layer CCA similarity with PET images (denoted by the orange curve), while the per-layer CCA similarity with the gray matter maps (denoted by the green curve) declines, suggesting that the tissue type information as the intermediary might not be enough to conclusively reason the transformation from T1-MR to PET. Inspired by the findings from previous medical researches [3,23] that certain brain regions (e.g., the basal ganglia, posterior cingulate cortex, and visual cortex) have variations in baseline glucose uptake, we propose our second hypothesis: there could be an in-between stage of identifying brain regions, followed by performing region-dependent transformation to infer the final PET image.

To verify this hypothesis, the per-layer CCA similarity scores with respect to brain region templates are computed, and are provided in Figure 3b. We observe that the translation model represents most of the brain region information in the bottleneck (i.e., from layer *actv9* to *actv12*). Remarkably, the per-layer CCA similarity scores with respect to the thalamus (denoted by the green curve) and putamen (denoted by the orange curve) are relatively high and sustained even in the late decoding stage, consistent with the finding that the thalamus and putamen have slightly higher metabolism activity [3]. To better understand the encoded brain region information in the translation model, the canonical components learnt from CCA are shown in Figure S2 of supplement. Intriguingly, from the visualization of layer *actv15* regarding the brain regions of caudate nucleus and putamen, we can observe co-occurrence of caudate nucleus and putamen in the feature space of the translation model. This echoes the well-documented fact that the caudate nucleus and putamen (which together are referred to as the striatum) act jointly in function as the major input zone for basal ganglia [5,6]. With the aforementioned analysis, we validate our second hypothesis that in the cross-modal medical image translation, there is likely an in-between stage of identifying and representing brain regions.

5 Explainable and Simplified Image Translation Model

Via CCA analysis, we validate our two main hypotheses that the translation from T1-MR images to PET ones includes the recognition of the brain tissues and regions. Yet, U-Net-based model comprises an entangled process of segmentation and transformation, it is challenging to further analyze the information related to brain tissue types and brain regions from the feature maps of the model.

To address such issue, we propose an Explainable and Simplified Image Translation (ESIT) model, where the information of the brain tissue types and

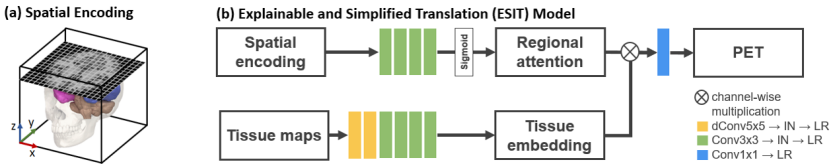

Fig. 4: (a) Illustration of the spatial encoding. (b) Overview of our Explainable and Simplified Image Translation (ESIT) model.

brain regions are explicitly unraveled and tackled in our model design. The architecture of our proposed ESIT model is illustrated in Figure 4. The ESIT model takes both the brain tissue maps and the spatial encoding as inputs. The spatial encoding is an $H \times W \times 3$ map that transforms the pixel coordinates of the T1-MR image (of size $H \times W$) into the universal brain coordinate system (as illustrated in Figure 4 (a)). In the ESIT model, the input map of spatial encoding is passed through several convolution layers and then becomes the *regional attention* map. On the other hand, the input tissue maps are transformed into the *tissue embeddings* by a shallow network. We integrate the regional attention maps and the tissue embeddings via channel-wise multiplication followed by a 1×1 convolution layer, then we obtain the final PET output. Simple as it may seem, our ESIT model attains competitive performance compared to the U-Net-based translation model (cf. Table S1 of supplement). Our ESIT provides a more straightforward and more explainable way to understand the underlying mechanism of T1-MR to PET image translation, which we will detail later.

5.1 Extraction of Regional Gray Matter Volume Information from Brain Tissue Maps

As our dataset comprises of images of subjects with a wide spectrum of clinical status, the good performance of deep models implies that the information of structural abnormality (e.g., gray matter volume, gray matter thickness) could be well extracted from the T1-MR images or brain tissue maps. Hence, we roll out experiments with a focus on the hippocampus and amygdala, the two brain regions susceptible to structural changes due to AD [4], to explore the associations between the tissue embeddings and the gray matter volume (obtained with Computational Anatomy Toolbox (CAT12) [7]) as well as the clinical status.

We visualize the tissue embeddings of the hippocampus and amygdala regions in Figure S3 of supplement, where we observe that the tissue embeddings are fairly likely to correlate with the gray matter volume as well as the clinical status of subjects in both areas. Such observation has its corresponding medical explanation: as PET is used to measure the brain metabolism (mostly synaptic activities [15]) and our tissue embeddings are contributing to the synthesis of PET images, the decrease in gray matter volume which reflects the loss of synapses and neurons can hence be captured by our tissue embeddings.

5.2 Regional Attention on Metabolic Variation in Aging and AD

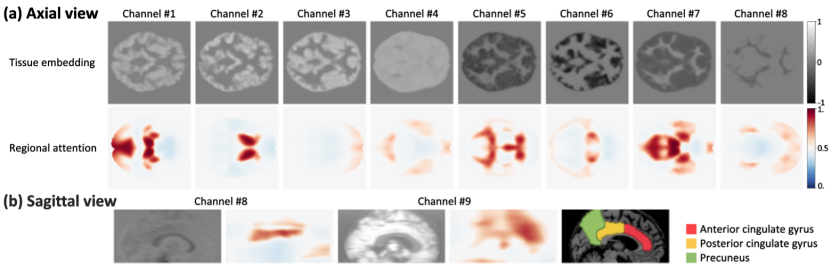

Fig. 5: The visualization of **(a) tissue embedding maps (top) and regional attention maps (bottom) learnt by our ESIT model, from axial view. (b) The tissue embeddings and regional attention maps from sagittal view**.

In this section, we revisit the brain region identification process using our proposed ESIT model, in which the regional information is processed independently such that we can focus more on the learnt regional patterns. In Figure 5, we show the learnt tissue embeddings as well as regional attention maps from axial and sagittal views. The tissue embeddings mostly follow the distribution of brain tissues and CSF. For regional attention maps, we summarize the four typical brain region patterns:

- *Regions with normal variation.* Channel #2 reveals the pallidum, caudate nucleus and putamen, all of which are the main components of the basal ganglia that have high metabolic activity in healthy population [3].
- *Regions with preserved metabolism during aging.* In channel #1, attention is given to the bilateral occipital lobes, thalamus, pallidum and heschl's gyrus, which are relatively unaffected during aging [3,12]. Likewise, channel #4 focuses on the superior frontal gyrus, superior temporal gyrus, and lingual gyrus, all of which has relatively preserved metabolism in aging population [12].
- *Aging-related regions.* Channel #9 mainly focuses on the anterior cingulate gyrus, the region with profound metabolic decrease during aging [16].
- *AD-related regions.* Channel #8 focuses on the posterior cingulate gyrus and precuneus regions, and both of them have the most reduction in glucose metabolism in subjects with AD [16,14,2].

These results show that our ESIT model identifies four typical patterns of regional hyper-metabolism or hypo-metabolism and thus reinforces our proposed hypothesis that there is region-dependent transformation for inferring the final PET images. We humbly conclude that the deep learning translation models are reasonably plausible from a medical perspective, where they learn to capture the characteristics of the regional metabolic differences such as normal regional variation, age-related change, and dementia-related regional alterations.

6 Conclusion

In this paper, we conduct extensive experiments using representational similarity to verify our proposed hypotheses that the translation from T1-MR to PET images comprises the recognition of brain tissue types and brain regions in its process, laying the explanatory groundwork for cross-modal medical image translation. Based on our findings, we propose a concise and more interpretable model, ESIT, and further demonstrate the capability of deep learning technique in extracting regional gray matter volume information and identifying the regional metabolic variation in normal, aging and dementia population.

References

1. Bach, S., Binder, A., Montavon, G., Klauschen, F., Müller, K.R., Samek, W.: On pixel-wise explanations for non-linear classifier decisions by layer-wise relevance propagation. PloS One (2015)
2. Bailly, M., Destrieux, C., Hommet, C., Mondon, K., Cottier, J.P., Beaufils, E., Vierron, E., Vercouillie, J., Ibazizene, M., Voisin, T., et al.: Precuneus and cingulate cortex atrophy and hypometabolism in patients with alzheimer's disease and mild cognitive impairment: Mri and 18f-fdg pet quantitative analysis using freesurfer. BioMed Research International (2015)
3. Berti, V., Mosconi, L., Pupi, A.: Brain: normal variations and benign findings in fluorodeoxyglucose-pet/computed tomography imaging. PET Clinics (2014)
4. Chételat, G., Desgranges, B., Landeau, B., Mézenge, F., Poline, J., de La Sayette, V., Viader, F., Eustache, F., Baron, J.C.: Direct voxel-based comparison between grey matter hypometabolism and atrophy in alzheimer's disease. Brain (2008)
5. Dale, P., George, A., David, F., Lawrence, K., Anthony-Samuel, L., James, M., S, W.: Neuroscience, 2nd edition. Sunderland (MA): Sinauer Associates (2001)
6. Driscoll, M.E., Bollu, P.C., Tadi, P.: Neuroanatomy, Nucleus Caudate. StatPearls Publishing, Treasure Island (FL) (2020)
7. Gaser, C., Dahnke, R.: Cat-a computational anatomy toolbox for the analysis of structural mri data. Human Brain Mapping (2016)
8. Hammers, A., Allom, R., Koepp, M.J., Free, S.L., Myers, R., Lemieux, L., Mitchell, T.N., Brooks, D.J., Duncan, J.S.: Three-dimensional maximum probability atlas of the human brain, with particular reference to the temporal lobe. Human Brain Mapping (2003)
9. Jack Jr, C.R., Bernstein, M.A., Fox, N.C., Thompson, P., Alexander, G., Harvey, D., Borowski, B., Britson, P.J., L. Whitwell, J., Ward, C., et al.: The alzheimer's disease neuroimaging initiative (adni): Mri methods. Journal of Magnetic Resonance Imaging (2008)
10. Lan, H., Toga, A., Sepehrband, F.: Sc-gan: 3d self-attention conditional gan with spectral normalization for multi-modal neuroimaging synthesis. bioRxiv:2020.06.09.143297 (2020)
11. Loshchilov, I., Hutter, F.: Decoupled weight decay regularization. In: International Conference on Learning Representations (ICLR) (2019)
12. Lowe, V.J., Weigand, S.D., Senjem, M.L., Vemuri, P., Jordan, L., Kantarci, K., Boeve, B., Jack, C.R., Knopman, D., Petersen, R.C.: Association of hypometabolism and amyloid levels in aging, normal subjects. Neurology (2014)

13. Manninen, S., Karjalainen, T., Tuominen, L., Hietala, J., Kaasinen, V., Joutsa, J., Rinne, J., Nummenmaa, L.: Cerebral grey matter density is associated with neuroreceptor and neurotransporter availability: A combined pet and mri study. bioRxiv:2020.01.29.924530 (2020)
14. Marcus, C., Mena, E., Subramaniam, R.M.: Brain pet in the diagnosis of alzheimer's disease. Clinical Nuclear Medicine (2014)
15. Márquez, F., Yassa, M.A.: Neuroimaging biomarkers for alzheimer's disease. Molecular Neurodegeneration (2019)
16. Mosconi, L.: Glucose metabolism in normal aging and alzheimer's disease: methodological and physiological considerations for pet studies. Clinical and Translational Imaging (2013)
17. Nie, D., Trullo, R., Lian, J., Petitjean, C., Ruan, S., Wang, Q., Shen, D.: Medical image synthesis with context-aware generative adversarial networks. In: International Conference on Medical Image Computing and Computer-Assisted Intervention (MICCAI) (2017)
18. Pan, Y., Liu, M., Lian, C., Zhou, T., Xia, Y., Shen, D.: Synthesizing missing pet from mri with cycle-consistent generative adversarial networks for alzheimer's disease diagnosis. In: International Conference on Medical Image Computing and Computer-Assisted Intervention (MICCAI) (2018)
19. Penny, W.D., Friston, K.J., Ashburner, J.T., Kiebel, S.J., Nichols, T.E.: Statistical parametric mapping: the analysis of functional brain images. Academic Press (2011)
20. Rolls, E.T., Huang, C.C., Lin, C.P., Feng, J., Joliot, M.: Automated anatomical labelling atlas 3. NeuroImage (2020)
21. Ronneberger, O., Fischer, P., Brox, T.: U-net: Convolutional networks for biomedical image segmentation. In: International Conference on Medical Image Computing and Computer-Assisted Intervention (MICCAI) (2015)
22. Selvaraju, R.R., Cogswell, M., Das, A., Vedantam, R., Parikh, D., Batra, D.: Grad-cam: Visual explanations from deep networks via gradient-based localization. In: IEEE Conference on Computer Vision and Pattern Recognition (CVPR) (2017)
23. Shamchi, S.P., Khosravi, M., Taghvaei, R., Zadeh, M.Z., Paydary, K., Emamzadehfard, S., Werner, T.J., Høilund-Carlsen, P.F., Alavi, A.: Normal patterns of regional brain 18f-fdg uptake in normal aging. Hellenic Journal of Nuclear Medicine (2018)
24. Shulman, R.G., Rothman, D.L., Behar, K.L., Hyder, F.: Energetic basis of brain activity: implications for neuroimaging. Trends in Neurosciences (2004)
25. Sikka, A., Peri, S.V., Bathula, D.R.: Mri to fdg-pet: cross-modal synthesis using 3d u-net for multi-modal alzheimer's classification. In: International Workshop on Simulation and Synthesis in Medical Imaging (2018)
26. Sun, H., Mehta, R., Zhou, H.H., Huang, Z., Johnson, S.C., Prabhakaran, V., Singh, V.: Dual-glow: Conditional flow-based generative model for modality transfer. In: IEEE International Conference on Computer Vision (ICCV) (2019)
27. Wei, W., Poirion, E., Bodini, B., Durrleman, S., Ayache, N., Stankoff, B., Colliot, O.: Learning myelin content in multiple sclerosis from multimodal mri through adversarial training. In: International Conference on Medical Image Computing and Computer-Assisted Intervention (MICCAI) (2018)
28. Yosinski, J., Clune, J., Nguyen, A., Fuchs, T., Lipson, H.: Understanding neural networks through deep visualization. ArXiv:1506.06579 (2015)
29. Zeiler, M.D., Fergus, R.: Visualizing and understanding convolutional networks. In: European Conference on Computer Vision (ECCV) (2014)